Universal Photonics Tomography

Prabhav Gaur[1]*, Andrew Grieco[1], Naif Alshamrani[1,2], Dhaifallah Almutairi[1,2], Yeshaiahu Fainman[1]

[1]Department of Electrical and Computer Engineering, University of California San Diego; 9500 Gilman Drive, La Jolla, CA 92093, USA.

[2]King Abdulaziz City for Science and Technology (KACST), P.O. Box 6086, Riyadh 11442, Saudi Arabia

*Corresponding author. Email: pgaur@eng.ucsd.edu

Abstract

3D imaging is essential for the study and analysis of a wide variety of structures in numerous applications. Coherent photonic systems such as Optical Coherence Tomography (OCT) and Light Detection and Ranging (LiDAR) are state of the art approaches, and their current implementation can operate in regimes that range from under a few millimeters to over more than a kilometer. We introduce a general method, which we call Universal Photonics Tomography (UPT), for analyzing coherent tomography systems, in which conventional methods such as OCT and LiDAR may be viewed as special cases. We demonstrate a novel approach based on the use of phase modulation combined with multirate signal processing to collect positional information of objects beyond the Nyquist limits. Depending on the location of the phase modulator in the system, and associated modulation scheme, we can improve the axial resolution or the maximum measurement distance (unambiguous range).

Introduction

Coherent signal processing is a powerful tool for real time 3D imaging of objects at distances ranging from a few hundred microns to several hundred meters with corresponding resolutions[1]. Optical Coherent Tomography (OCT)[2] is a well-developed imaging technique for objects at short distances with micron level resolution, hence is useful for various biomedical applications[3,4]. OCT has two different forms Time Domain OCT (TD-OCT) and Fourier Domain OCT (FD-OCT)[5]. The FD-OCT has been implemented exploiting two different approaches; the first one being Spectral Domain (SD-OCT) that utilizes a broadband source with spectrum analyzer. The second approach is the Swept Source (SS-OCT) that utilizes a tunable laser source combined with a photodetector. Among the different implementations, SS-OCT is the most promising, and can provide axial resolutions of 5 um and depth information up to a few millimeters[10]. Other variants of OCT such as Doppler OCT also exist for specialized applications where velocity measurement is also required[6].

For measurements of 3D objects at long distances ranging from a few meters to kilometers, a Light Detection and Ranging (LiDAR)[7,8] technique is employed using a modulated source and a photodetector. LiDAR has several applications, for example: surveying[9,10], forestry[11], atmospheric physics[12], and autonomous vehicles[13]. The most common scheme to implement LiDAR is by

measuring time of flight of pulsed lasers. A more recently developed technique is frequency modulated continuous wave LiDAR[8] (FMCW LiDAR) that uses a frequency chirp. The chirped signal is transmitted to the object and its replica is made to interfere with the returned signal, reflected from the object. The beat frequency is then used to determine the distance to the object. It is worth noting that the technique of SS-OCT and FMCW lidar resemble each other in terms of using a frequency sweep and measure distances using coherent detection[14]. The difference arises from the manner of frequency sweep, where in SS-OCT a particular frequency interferes with itself while in FMCW LiDAR different frequencies can interfere with each other due to time lag.

In this regard, it is possible to view these methods as part of a more general universal framework: a coherent interferometer that has the capability of optical modulation in different sections of the system. The prevailing techniques can all be viewed as special cases depending on the source, modulation format, and detection procedure. In one case, a laser, quadratic phase modulation and fast photodetector will implement FMCW LiDAR, whereas a frequency sweep and a slow photodetector becomes SS-OCT. According to conventional understanding, improvements to these technologies based on hardware have reached the point of diminishing returns[15]. Research has consequently shifted to alternative methods, such as superior processing algorithms, and complex modulation/detection schemes, in a bid to improve the resolution and depth performance[16-20].The primary advantage of this universal framework, which we call Universal Photonics Tomography (UPT), is that it can enable formulation of novel reconfigurable functionalities and capabilities to these existing techniques. In this work we demonstrate one such example, where the phase modulator in OCT can be exploited to scan multiple times and can be used to detect objects over longer distances by changing the resolution and depth parameters of the tomography system. These parameters are a direct consequence of Nyquist criterion with length (or time) and frequency forming Fourier pairs. They determine the limitations and effective cost of the system, and their relations are given by Eq. 1, where the axial resolution (l_o) is mainly determined by the bandwidth (B) of laser sweep while the maximum distance (L) by the frequency resolution (v_o).

$$l_o = c/B \quad ; \quad L = c/2v_o \tag{1}$$

Nearby object imaging is limited by the axial resolution l_0 (determined by the optical bandwidth) and far object imaging is limited by maximum distance L (determined by the frequency resolution). We mathematically develop this tomography system from first principles and show how the fundamental resolution and depth limitations can be pushed using phase modulation and multirate filter bank interpretation.

Results

Multirate filter banks are sets of filters, decimators and interpolators used widely in conventional digital systems[21]. Usually, decimators downsample the signal after passing through analysis filters. This compressed information is stored or transmitted via a channel. On the other end of channel, the signal is interpolated or upsampled and passed through synthesis filters to retrieve the original information. The process of downsampling means decreasing the resolution of system which is similar to an undersampled tomography system. The tomography systems are also discrete, and

analog filters can be implemented by phase modulation of the optical carrier signal and by digital processing after detection. Hence, the imaging system can be considered as multirate filter bank with each scanning cycle representing a single channel and carrying object information in a
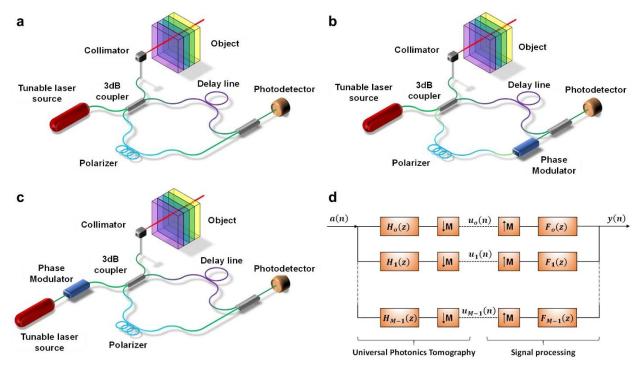

Fig. 1 | **Structure for Universal Photonics Tomography (UPT). a,** Base case: Setup for our implementation of UPT without phase modulators which resembles the Swept Source OCT in single mode fiber. **b,** First case: Phase modulator is added in the sample arm to the base case. A waveform generator (not shown) is used to give slow modulation which assists to improve the resolution in length domain. **c,** Second case: Phase modulator is added just after the tunable laser to the base case. A signal generator (not shown) is used to give fast modulation which assists to increase the maximum unambiguous range. **d,** Schematic for the working of UPT and the required post-processing in the filter bank form. The horizontal dashed lines indicate photodetection. The transfer functions are in frequency domain for the first case while in length (i.e., time) domain for the second case.

compressed form. Here, we demonstrate a 2-channel filter bank implementation which results in a twofold improvement in both length and frequency resolution of the tomography system. Using this scheme, both near and far objects as well as their density profiles can be measured with improved parameters. In this way it is more versatile than conventional approaches.

Formulation

I. Universal Photonics Tomography

The setup for our implementation of UPT, without the phase modulators, is shown in Fig. 1a. The normalized interference term (see Supplementary Information, S-I) measured at the photodetector is given by,

$$P_{intf}(k) = \sum_{i=-N}^{N} \bar{a}(i) \exp\left(\frac{j2\pi}{2N+1} ki\right) \tag{2}$$

where $\bar{a}(i)$ consists of reflection and transmission coefficients in the i-th surface present at a particular position with its magnitude determined from Fresnel equations[22] and the transmitted optical power to the object, N is the total number of surfaces present, and each value of k represents a frequency in laser sweep. The negative arguments of the summation represent the conjugate part of the interference. $\bar{a}(i)$ can be obtained by taking the Discrete Fourier Transform (DFT) of P_{intf}. The position, i, of the non-zero elements of $\bar{a}(i)$ give the optical distance of the surface, while their magnitude can be used to determine the optical index of the layer which in turn can be used to extract the true physical distance.

II. Frequency dependent slow modulation

Next we add a phase modulator to the sample arm and use a signal generator, as shown in Fig. 1b, to introduce a phase modulation $\phi(t)$. Assuming that the modulation is slow compared to the time taken (time bin) by the laser to measure a single frequency, the DFT (transformation from k to n) of the interference term (P_{intf}) is given by,

$$2N\, \mathcal{F}[P_{intf}(k)](n) = |F|^2 a(n) * h(n) + |F|^2 a^*(-n) * h^*(-n) \tag{3}$$

where $|F|^2 a(n) = \bar{a}(i)$ for $n > 0$ and $|F|^2$ is the transmitted optical power to the object. $h(n) = \mathcal{F}[\exp(j\phi(k\Delta t))]$, where $\mathcal{F}[.]$ is the DFT function and Δt (time bin) is the time taken to measure the power at a single frequency. Eq. 3 can be truncated to $n > 0$ regime and then normalized by $|F|^2$ to give $u(n)$ (see Supplementary Information, S-II).

$$u(n) = a(n) * h(n) \tag{4}$$

Eq. 4 resembles a filter $h(n)$ applied to $a(n)$ in a linear system with convolution in length (i.e., time) domain. A transfer function can then be defined in frequency domain, and this provides the opportunity to apply digital signal processing on the depth information.

III. Frequency independent fast modulation

In this case, we place the phase modulator just after the laser, as shown in Fig. 1c. We use fast modulation which repeats after every sweep frequency i.e., it is periodic with Δt. It can then be shown that the interference term is given by,

$$P_{intf}(k) = \sum_{i=-N}^{N} \bar{a}(i)\bar{H}(i) \exp\left(\frac{j2\pi v_o l_o ki}{c}\right) \tag{5}$$

where $\bar{H}(i)$ is the autocorrelation function of the phase modulation (see Supplementary Information, S-III). Eq. 5 can be written in the convolution form.

$$u(n) = \tilde{a}(n) * h(n) \tag{6}$$

Here the P_{intf} has been replaced by $u(n)$ and variable k is replaced n. $\tilde{a}(n) = \mathcal{F}[\bar{a}(i)]$, and $h(n) = \mathcal{F}[\bar{H}(i)]$ determines the filter coefficients (see Supplementary Information, S-III). Note that here the convolution is in frequency domain, as opposed to previous case. Hence, the transfer function can be implemented in length domain.

IV. Multirate Filter Bank

Eq. 4 and Eq. 6 represents a linear system in which multirate signal processing can be used to increase the resolution of the system as shown in Fig. 1d. By performing multiple scans, axial resolution is improved in the first case while maximum depth is increased in the second case. The first case may arise when bandwidth of laser is limited while second case may arise when frequency resolution is limited. These two cases are equivalent to the presence of a downsampled block in the system. Analysis filters are implemented using phase modulators while the synthesis filters and upsampling blocks are implemented digitally. In the result section, we demonstrate a 2-channel filter bank for both the cases.

For slow modulation we use a linear phase modulation, which is effectively a z^{-1} transfer function in Z domain (see Supplementary Information, S-IV). This results in a lazy-filter bank. For fast modulation, sinusoids are the only cost-effective option. The transfer function then corresponds to a Bessel function (first kind, zeroth order) of a sinusoid (see Supplementary Information, S-IV).
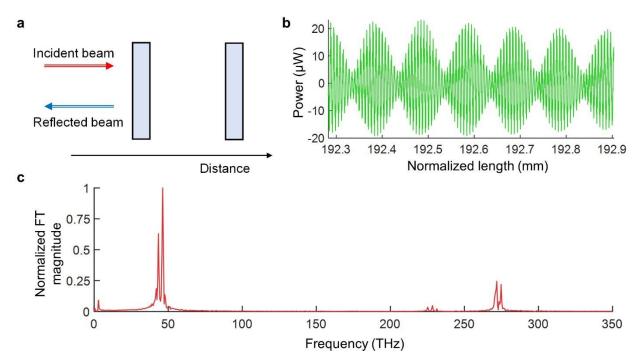

Fig. 2 | **Experimental demonstration of UPT without modulators (Base Case). a,** The objects used are a couple of microscope slides placed one behind the other. **b,** The measured interference pattern on the photodetector as a function of frequency sweep. **c,** Fourier transform (FT) of the interference pattern. The four larger peaks predict the distances of the surfaces present. The smaller peaks (barely visible) are due to autocorrelation of the sample arm signal in the interferogram and can be removed by balanced photodetection.

The synthesis filters can be calculated from the perfect reconstruction conditions of filter banks, as given by Eq. 7 and Eq. 8. K is an integer and corresponds to the delay due to signal processing.

$$\begin{bmatrix} F_o(z) \\ F_1(z) \end{bmatrix} = \frac{2z^{-K}}{\Delta(z)} \begin{bmatrix} H_1(-z) \\ -H_o(-z) \end{bmatrix} \tag{7}$$

$$\Delta(z) = H_o(z)H_1(-z) - H_o(-z)H_1(z) \tag{8}$$

Experimental Results

The results demonstrate the working principal of the device, which is developed in the section above, under the universal framework. We then experimentally demonstrate how various modulation schemes provides the opportunity for novel detection and post-processing strategies.

I.   Universal Photonics Tomography

To demonstrate the UPT, we use two microscope slides as objects (Fig. 2a), one placed directly in front of the other, hence a total of four different interface surfaces separating two different media (namely air and glass). The microscope slides are about 1mm thick, and the two slides are placed about 12 cm apart. The refractive index of glass is assumed to be $n_{glass} \approx 1.5$, and the refractive index of air is taken to be $n_{air} \approx 1.0$. Fig. 2b shows the detected interferogram after using an offset equal to its mean. The bandwidth is 5 nm at a wavelength of 1.55 µm and resolution (v_o) is 0.3 pm. As shown in Fig. 2c, the Fourier transform clearly distinguishes the four surfaces and gives accurate distances of all surfaces.

II.   Increasing Axial Resolution

To demonstrate how to increase the axial resolution we use a microscope slide and a mirror behind it, as shown in Fig. 3a. We create a situation where the bandwidth of laser is not high enough to clearly distinguish the two surfaces of the slide. The laser sweeps a bandwidth of 1 nm with 0.2 pm resolution. This results in an axial resolution (l_o) of 2.4 mm, while the normalized distance between the slide surfaces is 3 mm. This measurement referred to as unmodulated signal, (curve Ch 0 in Fig. 3b, green curve and Fig. 3d green curve) corresponds to conventional SS-OCT, but the surfaces are barely resolvable due to limited bandwidth of the tunable laser source. . Next, we use a waveform generator to provide a linear phase modulation to the sample arm, as shown in Fig. 3c. The interferogram that is obtained can distinguish the surfaces better or worse depending on the position of surfaces, but the resolution (l_o) remains the same (Fig. 3b blue curve and Fig. 3d blue curve). Now we combine the two signals, treating them as two different channels of a multirate filter bank (Fig. 3e). This improves l_o from 2.4 mm to 1.2 mm. The surfaces can be distinguished much more easily now, and their position are known twice more accurately than before. Hence the axial resolution of the synthesized signal with a 1 nm bandwidth optical source is equal to that of a single channel system with a 2 nm source, a 100% improvement! Further, note that multiple channels can be used to improve the axial resolution even more. This is a highly significant result, as it provides the best path to ultrahigh resolution devices by a large margin.
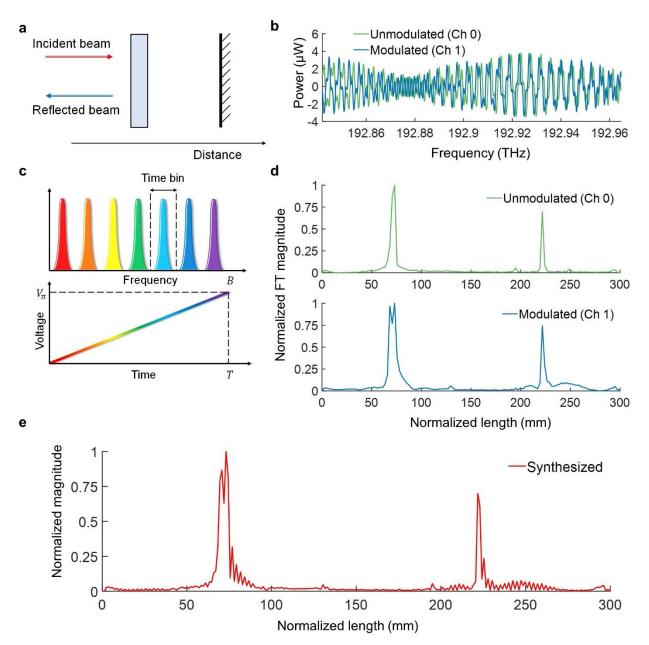
Fig. 3 | Demonstration of UPT for increasing axial resolution (First Case). a, The objects are a microscope slide and a mirror with the former in front of the later. **b,** The measured interference pattern of the unmodulated channel 0 (green curve) and modulated channel 1 (blue curve) as function of frequency. **c,** Schematic of the linear modulation given to Channel 1 (Ch 1). **d,** Fourier transform (FT) of Ch 0 (green curve) and Ch 1 (blue curve). **e,** Synthesized distance estimation of the objects by combining both the channels as part of a lazy-filter bank. The resulting curve has twice better length resolution compared to the ones detected in the individual channels.

III. Increasing Maximum Depth

For a simple demonstration on how to increase the maximum unambiguous depth, we again use the microscope slide with a mirror behind it (see Fig. 3a). We define a balanced point which is the zero position in the length domain and physically represents the point where delay of reference signal is equal to that of signal from the object. The microscope slide is used as a reference, which
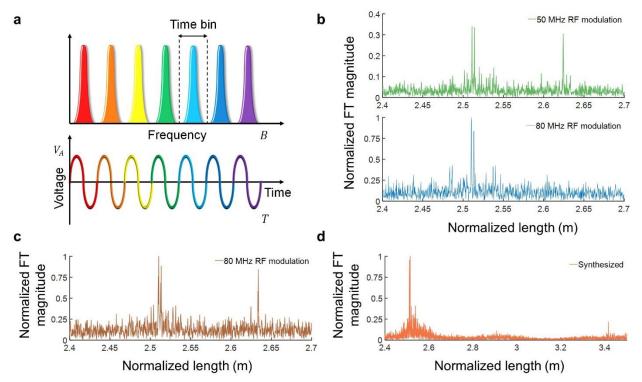
Fig. 4 | Demonstration of UPT for increasing maximum unambiguous depth (Second case). a, Schematic depicting the voltage applied to phase modulation as laser frequency is tuned. **b,** Fourier transform of the measured power when phase modulator is given 50 MHz sinusoidal signal at channel 0 (green curve) and 80 MHz sinusoidal signal at channel 1 (blue curve). These both are combined to predict the true position of the mirror, which is beyond the Nyquist limit **c,** Fourier transform of the measured power when a mirror is actually placed in the aliased position of the original mirror. Comparing the 80 MHz RF modulation between the blue and brown curves show the effect of length dependent transfer function that differently affects the two peaks that are at different physical positions, even though they show up at the same place in Fourier domain due to aliasing. **d,** Synthesized signal by combining the two channels and passing them through the synthesis filters. The peak at 3.41 m predict the true position of the mirror.

is at 2.51 m from the balanced point, while the mirror, which is at 3.41 m from the balanced point, is the target object. Here we consider the situation when the resolution of laser sweep is limited to 0.4 pm, which corresponds to maximum unambiguous depth (L) equal to 3 m, and the position of the target (mirror) is beyond it. We first measure this object with 50 MHz sinusoidal phase modulation as shown in Fig. 4b green curve. The peak for mirror appears at 2.62 m which is an aliasing artifact that arises due to undersampled measurement. To predict the true position of the target we perform a second measurement where the transfer function of the phase modulation has a zero at the unaliased position of the target but not at the aliased position. If the target peak disappears then it indicates that the target is indeed at much further distance, otherwise the original peak gives the correct position. Thus, we use adaptive phase modulation and signal processing to determine the position of a single target which is often the requirement of a conventional LiDAR system. This is a valuable method as it is often difficult to determine the accurate transfer function of the optical modulation due to nonlinearity, variable V_π , RF impedance mismatch, etc., but this method only requires the knowledge of zero crossings of the transfer function. In our case, an 80 MHz sinusoidal phase modulation gives a transfer function that has a zero at 3.41 m and we show that this makes the 2.62 m peak disappear (Fig. 4b blue curve). Therefore, we can conclude that

position of the target is actually at 3.41 m. We also demonstrate in Fig. 4c that the peak would not have disappeared if the true position of the mirror were actually at 2.62 m, by physically placing a mirror at this position. Also, the 50 MHz and 80 MHz measurements can be treated as two different channels in a multirate filter bank and combined, as shown in Fig. 4d, to give a graph that has twice the maximum unambiguous range than individual channels. This method will perform better for more complex objects but also require an accurate structure of the analysis of the transfer function produced by phase modulation (see Supplementary Information, S-IV). Hence, we showed that distances up to 6 m can be measured by using laser sweep resolution which corresponds to only maximum depth of 3 m in the unmodulated case. As mentioned above, multiple channels (scans) can be used to increase the limit even more. Also, for simple targets, adaptive measurements can be performed which will require lesser number of channels and can still measure much farther positions of the target. This is a highly significant result for the same reasons.

Discussion

We have demonstrated UPT which is a universal method to measure depth and position of objects at various distances by adjusting the laser sweep frequency and bandwidth. We implemented a system, that validates the SS-OCT as a special case under the UPT framework, which is limited in depth by the tuning frequency resolution of the laser, and which is limited in spatial resolution by the bandwidth of the laser. In this case, improving the performance of the device would necessitate simultaneously increasing the tunable bandwidth of the laser, as well as the tuning resolution, while also increasing the output power so the spectral power density is maintained. This is an uneconomical prospect at best. The bandwidth and frequency resolution of a tunable laser is limited by size, power, material properties, etc.[23,24]. Improving them directly will make the system bulky, cost ineffective and difficult to implement. As an alternative, we used the UPT framework to design and demonstrate an alternative approach that improves the resolution and depth performance through the use of slow and fast modulation of the optical carrier. This only requires a simple phase modulator and waveform/signal generator which are far more economical and much easier to integrate in the system. By making multiple scans, ultrahigh resolutions can be achieved both in frequency and length domain. The only drawback in this method is the extra time taken to perform multiple scans. The design is agnostic to the type of phase modulators used, which can be mechanical, acousto-optic, electro-optic, etc. In our experiments, we used Lithium Niobate phase modulators[25] which have promising specifications of low V_π and high RF bandwidths.

This multichannel detection scheme has no theoretical limit. But for long distances the detected power might drop below the noise levels of the photodetectors. Another practical challenge exist is the imprecision in the frequency sweep. If all the frequency values reported by the laser do not have constant frequency difference, the Fourier transform will be noisy when making a measurement near or beyond the Nyquist limit. We observe this in the second case where the noise floor is due to the improperly spaced frequency values. The power on the photodetector comprises of the DC term (reference autocorrelation), the sample autocorrelation and the interference term (cross-correlation). To efficiently extract the interference term with high SNR, it is important to filter out the remaining two terms. One way is to attenuate the signal in the sample arm and subtract

the mean of the total interference power. This method can still produce small peaks in the Fourier transform due to presence of autocorrelation term, which can also be observed in our base case (Fig. 2). The better way to remove the other two terms is using balanced photodetection, where subtracting the two interference powers cancels out the two unnecessary terms.

To implement synthesis filters, it is essential that $\Delta(z)$ as described in Eq. 8 is invertible. This is not the case when sinusoidal phase modulation is given to only to one channel with no modulation on the other. Hence, for second case, both channels should have sinusoidal modulation. Other modulation shapes can also be used if the speed of waveform generator permits. Under the UPT framework other novel configurations are also possible, for example, using intensity modulators instead of phase modulators to implement more complex filters, or developing the system similar to SD-OCT and using optical modulation to virtually improve the bandwidth of the source and frequency resolution of the spectrum analyzer.

From an engineering standpoint the most significant results are the improvements in axial resolution and maximum depth measurement without increasing the signal bandwidth and frequency resolution of tunable laser. This is because many factors form a hard limit on the source bandwidth in conventional systems. Specifically, these include source limitations, transparency windows of the optical components, and power tolerance. Similarly, frequency resolution is limited by factors depending on the tunable laser, for example, external cavity lasers require large cavities for small free spectral range. Operation under the UPT framework bypasses all these hardware challenges without the use of exotic and costly equipment.

References

1. Tan, A C S et al. An overview of the clinical applications of optical coherence tomography angiography. *Eye (London, England)* vol. **32**,2 (2018).

2. Huang, D. et al. Optical coherence tomography. *Science (New York, N.Y.)* vol. **254**,5035 (1991): 1178-81.

3. Huemer, J. et al. Phenotyping of retinal neovascularization in ischemic retinal vein occlusion using wide field OCT angiography. *Eye (London, England)*, 10.1038/s41433-020-01317-9. 30 Nov. 2020.

4. Trichonas, G., & Kaiser, P. K. (2014). Optical coherence tomography imaging of macular oedema. *The British journal of ophthalmology*, **98** Suppl 2(Suppl 2), ii24–ii29.

5. Leitgeb, R., Hitzenberger, C., & Fercher A.Performance of fourier domain vs. time domain optical coherence tomography," *Opt. Express* **11**, 889-894 (2003).

6. Bhende, M., Shetty, S., Parthasarathy, M. K., & Ramya, S. (2018). Optical coherence tomography: A guide to interpretation of common macular diseases. *Indian journal of ophthalmology*, **66**(1), 20–35.

7. Dong, P., & Chen, Q. (2017). *LiDAR Remote Sensing and Applications (1st ed.)*. CRC Press. Boca Raton.

8. Behroozpour, B., Sandborn, P. A. M., Wu, M. C. & Boser, B. E. Lidar System Architectures and Circuits. *IEEE Communications Magazine*, vol. **55**, no. 10, pp. 135-142, Oct. 2017.

9. Behrenfeld, M. et al. Annual boom–bust cycles of polar phytoplankton biomass revealed by space-based lidar. *Nature Geosci* **10**, 118–122 (2017).

10. Inomata, T. et al. Monumental architecture at Aguada Fénix and the rise of Maya civilization. *Nature* **582**, 530–533 (2020).

11. Dalagnol, R. et al. Large-scale variations in the dynamics of Amazon forest canopy gaps from airborne lidar data and opportunities for tree mortality estimates. *Sci Rep* **11,** 1388 (2021).

12. Panahifar, H., Moradhaseli, R. & Khalesifard, H.R. Monitoring atmospheric particulate matters using vertically resolved measurements of a polarization lidar, in-situ recordings and satellite data over Tehran, Iran. *Sci Rep* **10,** 20052 (2020).

13. LiDAR drives forwards. *Nature Photon* **12,** 441 (2018).

14. Okano, M. & Chong, C. Swept Source Lidar: simultaneous FMCW ranging and nonmechanical beam steering with a wideband swept source. *Opt. Express* **28**, 23898-23915 (2020).

15. Aumann, S., Donner, S., Fischer, J., Müller, F. (2019) Optical Coherence Tomography (OCT): Principle and Technical Realization *High Resolution Imaging in Microscopy and Ophthalmology: New Frontiers in Biomedical Optics*, edited by Josef F. Bille, Springer, 14 August 2019.pp. 59–85.

16. Werkmeister, René M et al. "Ultrahigh-resolution OCT imaging of the human cornea." *Biomedical optics express* vol. **8**,2 1221-1239. 30 Jan. 2017.

17. Wang, T., Chan, M., Lee, H., Lee, C., & Tsai, M. Ultrahigh-resolution optical coherence tomography/angiography with an economic and compact supercontinuum laser. *Biomedical optics express* vol. **10**,11 5687-5702. 11 Oct. 2019.

18. Du, B. et al. High-speed photon-counting laser ranging for broad range of distances. *Sci Rep* **8**, 4198 (2018).

19. Kuse, N. & Fermann, M. E. Frequency-modulated comb LIDAR. *APL Photonics* **4**, 106105 (2019).

20. Kim, T., Bhargava, P. & Stojanovic, V. Optimal Spectral Estimation and System Trade-Off in Long-Distance Frequency-Modulated Continuous-Wave Lidar. *2018 IEEE International Conference on Acoustics, Speech and Signal Processing (ICASSP)*, Calgary, AB, Canada, 2018, pp. 1583-1587.

21. Zuluaga, J. R. & Naredo, J. L. Poly-phase filter-bank realization for the simulation of electric-network transients. *2014 11th International Conference on Electrical Engineering, Computing Science and Automatic Control (CCE)*, 2014, pp. 1-6.

22. Gupta, P., Pandey, A., Vairagi, K. & Mondal, S. K. Solving Fresnel equation for refractive index using reflected optical power obtained from Bessel beam interferometry. *Review of Scientific Instruments* **90**, 015110 (2019).

23. Liu, L., Li, Y. & Li, X. A broadband tunable laser design based on the distributed Moiré-grating reflector. *Optics Communications* vol. **458**, 2020.

24. Duarte, F.J. (2013). *Tunable Laser Optics (2nd ed.)*. CRC Press, Boca Raton

25. Ren, T. et al. An Integrated Low-Voltage Broadband Lithium Niobate Phase Modulator. *IEEE Photonics Technology Letters*, vol. **31**, no. 11, pp. 889-892, 1 June1, 2019.

Methods

Universal Photonics Tomography

The laser used for performing all the experiments is the 81608A Tunable Laser Source from Keysight which can give frequency resolution up to 0.1 pm and has a narrow linewidth (<10 kHz). The photodetector is the 81635A Dual Optical Power Sensor, also from Keysight. The phase modulator employed in both the cases is the Thorlabs Lithium Niobate 40 GHz phase modulators (LN27S-FC). The linear waveform is produced using Keysight B2960 series power supply while the sinusoidal signal is generated using Keysight MXG series 6 GHz Analog Signal Generator. The entire setup (excluding objects) is built upon SMF-28 single mode fiber.

Acknowledgements

Author contributions

A.G. and Y.F. conceived and supervised the project. P.G. and A.G. developed and analyzed the mathematical model, and designed the experimental setup. P.G. performed the simulations, wrote the signal processing code and realized the experiments. N.A. and D.A. contributed to the mathematical model and the experimental setup. All authors contributed to discussing the results and preparing the manuscript.

Supplementary Information

S-I. Universal Photonics Tomography

In this supplementary material, we use complex field to model signals at various parts in the system. First, we consider the field that is reflected from an object whose position and depth is under investigation. Then we look at the interference of this reflected signal with a reference signal. Initially, the base case without any phase modulator is formulated and it is shown how the discrete Fourier transform of frequency sweep gives positional information of the object. Later we discuss the effect of phase modulator at two different positions.

Consider a heterogenous object with multiple optical media and their corresponding surface present only at an effective optical distance of il_o from the first surface. Since a reflected beam will pass through each section twice (once in the transmission direction, and once in the reflected direction), the effective optical path length of each section is defined as twice the distance multiplied by the effective index of the medium. i is an integer in $[1, N\text{-}1]$. l_o determines the axial resolution of the imaging system. A complex field F, with a certain carrier frequency v, is incident on this sample. The reflection from the ith surface is given by equation (1).

$$r_i = a(i)F\exp(j\Phi_i) \tag{9}$$

a is a vector with reflection coefficients from each surface as its components. The reflection coefficient can be calculated from Fresnel equations. In theory, $a(i)$ can have contributions from surfaces other than the ith surface. This is because of multiple reflection in between the surfaces that give the same delay as the ith surface would have produced. But these extra terms can be neglected because usually r (reflection coefficient) $\ll t$ (transmission coefficient) which will attenuate the multiple reflections. If i^{th} surface is absent the $a(i)$ can be considered to be zero. Φ_i is the phase accumulated depending over the effective length and the carrier frequency v. Scattering is neglected to keep the formulation simple. The total reflection coming from the object is given by equation (2)

$$r_{total} = \sum_{i=1}^{N} r_i \tag{10}$$

The field in the sample arm will be proportional to r_{total}. The proportionality constant depends on 1) coupling coefficient of the 3db fiber coupler, losses, etc. which are neglected as they are scaling terms, and 2) sample arm length, which is assumed to be equal to that of reference arm and is also neglected.

$$r_{sample} = \sum_{i=1}^{N} a(i)F\exp(j\Phi_i) \tag{11}$$

The field in the reference arm is given by equation (4).

$$r_{reference} = F \tag{12}$$

Let P be the power detected by the photodetector.

$$P = \langle |r_{sample} + r_{reference}|^2 \rangle \tag{13}$$

The interference term is given by equation (6).

$$P_{intf} = |F|^2 \left\langle \sum_{i=1}^{N} a(i) \exp(j\Phi_i) + \sum_{i=1}^{N} a^*(i)F \exp(-j\Phi_i) \right\rangle \tag{14}$$

$\langle - \rangle$ is the time average. Assume a new set of phases with mapping $\Phi_i \rightarrow \Phi_i$ for $i > 0$, $-\Phi_{-i} \rightarrow \Phi_i$ for $i < 0$ and $\Phi_0 = 0$. Also mapping $a(i) \rightarrow \hat{a}(i)$ for $i > 0$, $a^*(-i) \rightarrow \hat{a}(i)$ for $i < 0$ and $\hat{a}(0) = 0$.

$$P_{intf} = |F|^2 \left\langle \sum_{i=-N}^{N} \hat{a}(i) \exp(j\Phi_i) \right\rangle \tag{15}$$

The effective distance between the 1st and i^{th} surface (as defined before) is il_o for $i > 0$. Performing mapping for Φ_i as above, it can be shown that equation (8) holds for all possible values of i.

$$\Phi_i = \frac{2\pi v l_o i}{c} \tag{16}$$

As the light reflected from i^{th} surface will be delayed by $\frac{l_o i}{c}$ the integration time at the photodetector will keep reducing as surfaces gets farther. Assuming Δt to be time for which the laser is active for a given frequency

$$P_{intf} = |F|^2 \sum_{i=-N}^{N} \int_{\frac{l_o i}{c}}^{\Delta t} \hat{a}(i) \exp\left(\frac{j2\pi v l_o i}{c}\right) dt \tag{17}$$

It is safe to assume that $\frac{l_o N}{c} \ll \Delta t$ as time taken by the system to measure one frequency ($\sim$100 µs) is significantly less than the time taken by light to travel as long as a kilometer ($<$5 µs). Also, the area of the integral and $|F|^2$ can be normalized with $\hat{a}(i)$ resulting in $\bar{a}(i)$

$$P_{intf} = \sum_{i=-N}^{N} \bar{a}(i) \exp\left(\frac{j2\pi v l_o i}{c}\right) \tag{18}$$

For a swept laser, we can measure discrete frequencies. As we have $2N + 1$ terms in the summation, we measure the interference term at $2N + 1$ frequencies with resolution v_o. For an integer k in $[0,2N]$

$$v = v_o k \tag{19}$$

To comply with the Nyquist sampling condition, the frequency resolution is chosen such that $\frac{v_o l_o}{c} = \frac{1}{2N+1}$ and the laser measures at $2N + 1$ points. Then the discretized version of interference term is given by equation (12).

$$P_{intf}(k) = \sum_{i=-N}^{N} \bar{a}(i) \exp\left(\frac{j2\pi}{2N + 1} ki\right) \tag{20}$$

Equation (12) represents the inverse Discrete Fourier Transform between the measured power and reflection coefficients. Taking $2N + 1$ point DFT of P_{intf} give back the information on the object. Note

that only the positive part of $\bar{a}$ is needed to obtain a. The position of non-zero elements of a give the optical distance of the surface, while their magnitude can be used to determine the optical index of the layer which in turn can be used to extract the true physical distance.

S-II. Frequency dependent slow modulation

Now, described as first case, we add a phase modulator to the sample arm and use a waveform generator to give a phase modulation $\phi(t)$. The modulation given here is slow and is assumed to be constant during Δt, the time during which laser is active and the photodetector integrates for a particular frequency in the same time period. This makes the phase modulation act like a filter as shown below.

In addition to the base case, the field in the sample arm has an extra phase modulation term and is given by equation (13).

$$r_{sample} = \sum_{i=1}^{N} a(i)F \exp(j\Phi_i) \exp(j\phi(t)) \tag{21}$$

The interference term is then given by equation (14).

$$P_{intf} = |F|^2 \langle \sum_{i=1}^{N} a(i) \exp(j\Phi_i) \exp(j\phi(t)) + \sum_{i=1}^{N} a^*(i)F \exp(-j\Phi_i) \exp(-j\phi(t)) \rangle \tag{22}$$

As the modulation depends on time, which also governs the carrier frequency, the time integration limits are frequency dependent.

$$\begin{aligned} P_{intf}(k) = |F|^2 \sum_{i=1}^{N} \int_{k\Delta t+\frac{l_o i}{c}}^{(k+1)\Delta t} a(i) \exp\left(\frac{j2\pi v_o l_o ki}{c}\right) \exp(j\phi(t)) \ dt \\ + |F|^2 \sum_{i=1}^{N} \int_{k\Delta t+\frac{l_o i}{c}}^{(k+1)\Delta t+\frac{l_o i}{c}} a^*(i) \exp\left(\frac{-j2\pi v_o l_o ki}{c}\right) \exp(-j\phi(t)) \ dt \end{aligned} \tag{23}$$

If $\phi(t)$ is slowly varying in Δt and $\frac{l_o N}{c} \ll \Delta t$

$$\begin{aligned} P_{intf}(k) = |F|^2 \sum_{i=1}^{N} a(i) \exp\left(\frac{j2\pi v_o l_o ki}{c}\right) \exp(j\phi(k\Delta t)) \\ + |F|^2 \sum_{i=1}^{N} a^*(i) \exp\left(\frac{-j2\pi v_o l_o ki}{c}\right) \exp(-j\phi(k\Delta t)) \end{aligned} \tag{24}$$

As $a(i)$ is single sided, we can assume $a(i) = 0$ for $-N + 1 \leq i \leq 0$.

$$P_{intf}(k) = |F|^2 \sum_{i=-N+1}^{N} a(i) \exp\left(\frac{j2\pi v_o l_o ki}{c}\right) \exp\left(j\phi(k\Delta t)\right)$$

$$+ |F|^2 \sum_{i=-N+1}^{N} a^*(i) \exp\left(\frac{-j2\pi v_o l_o ki}{c}\right) \exp\left(-j\phi(k\Delta t)\right)$$

<div align="right">(25)</div>

Let $\tilde{H}(k) = \exp\left(j\phi(k\Delta t)\right)$ and the $2N$ point DFT of $\tilde{H}(k)$ be $h(n)$. For satisfying Nyquist criterion we should have $\frac{v_o l_o}{c} = \frac{1}{2N}$ and laser must sweep over $2N$ points. Taking $2N$ DFT on both side

$$2N\, \mathcal{F}[P_{intf}(k)](n) = |F|^2 a(n) * h(n) + |F|^2 a^*(-n) * h^*(-n)$$

<div align="right">(26)</div>

If $h(n)$ is base limited and its support is very small compared to $2N$, the second term is negligible for $n > 0$. Hence the length domain information is truncated to N points. No information is lost in this process as N points are enough to get all information on $a(n)$, similar to the case without modulation. This truncated signal can be normalized and given by $u(n)$.

$$u(n) = a(n) * h(n)$$

<div align="right">(27)</div>

Now taking the Z-transform on both sides

$$U(z) = A(z)H(z)$$

<div align="right">(28)</div>

The capital letters U, A and H in the above equation are Z-transform of their corresponding small letter. Hence, phase modulation can be interpreted as a transfer function and $A(z)$ can be obtained back by dividing $U(z)$ by $H(z)$.

S-III. Frequency independent fast modulation

Now, described as second case, we place the phase modulator just after the laser, and provide a modulation $\phi(t)$ that is fast when compared to Δt and its time period is comparable to time equivalent length resolution l_o/c. Also, this modulation repeats after every sweep frequency. We consider the interference term again as done previously and formulate how phase modulation again becomes a filter but with inverted domain compared to the first case.

Considering interference term in this case, equation (15) thus becomes equation (21)

$$P_{intf}(k) = |F|^2 \sum_{i=1}^{N} \int_{\frac{l_o i}{c}}^{\Delta t} a(i) \exp\left(\frac{j2\pi v_o l_o ki}{c}\right) \exp\left(j\phi\left(t - \frac{l_o i}{c}\right)\right) \exp\left(-j\phi(t)\right)\, dt$$

$$+ |F|^2 \sum_{i=1}^{N} \int_{\frac{l_o i}{c}}^{\Delta t} a^*(i) \exp\left(\frac{-j2\pi v_o l_o ki}{c}\right) \exp\left(-j\phi\left(t - \frac{l_o i}{c}\right)\right) \exp\left(j\phi(t)\right)\, dt$$

<div align="right">(29)</div>

Define the auto-correlation function $\bar{H}(i)$ such that

$$\bar{H}(i) = \begin{cases} \dfrac{1}{\Delta t} \displaystyle\int_0^{\Delta t} \exp\left(j\phi\left(t - \dfrac{l_o i}{c} \right) \right) \exp\big(-j\phi(t)\big)\, dt \; ; & i > 0 \\[10pt] 1 & ; \quad i = 0 \\[10pt] \dfrac{1}{\Delta t} \displaystyle\int_0^{\Delta t} \exp\left(-j\phi\left(t - \dfrac{l_o i}{c} \right) \right) \exp\big(j\phi(t)\big)\, dt \; ; & i < 0 \end{cases} \tag{30}$$

Also defining $\bar{a}(i)$ as before

$$P_{intf}(k) = \sum_{i=-N}^{N} \bar{a}(i)\bar{H}(i) \exp\left(\frac{j2\pi v_o l_o ki}{c} \right) \tag{31}$$

Similar to before, $\frac{v_o l_o}{c} = \frac{1}{2N+1}$ and laser sweeps to $2N + 1$ points. Let $\tilde{a}(n)$ and $h(n)$ be the $2N + 1$ point DFT of $\bar{a}(i)$ and $\bar{H}(i)$ respectively. Changing the variable from k to n and P_{intf} to u

$$u(n) = \tilde{a}(n) * h(n) \tag{32}$$

Note that equation (19) and equation (24) look same, but the former is convolution in length domain while the latter in frequency domain. Hence, the interpretation of transfer function will be domain inverted compared the previous case. Taking the Z -transform results in

$$U(z) = A(z)H(z) \tag{33}$$

S-IV Multirate Filter Bank

Equation (20) corresponds to a transfer function block with the Z-transform in frequency domain. As the maximum bandwidth of the laser is usually limited, it may cause the resolution in length domain (axial resolution) to be less than desired, resulting in under sampling. Let the laser have a bandwidth that is M times smaller than required so that the axial resolution is down sampled by a factor of M from the desired l_o. This can be depicted by a block diagram as shown in fig. 1d main. The block diagram resembles a single channel of M channel filter bank. If we make the measurement M times with M different synthesis filters (H_m), the ideally sampled signal can be reconstructed using analysis filters (F_m). On the other hand, equation (25) corresponds to a transfer function block with the Z-transform in length domain. The same multirate filter bank analysis can be used to deal with under sampling problem. In this case, downsampling is in frequency domain as the resolution of sweeping laser is limited. Hence, the filter bank can be used to reconstruct the signal with increased frequency resolution and detect object at greater depth without aliasing.

For demonstration purpose we discuss the situation when M=2. The perfect reconstruction (PR) of $a(n)$ is said to be achieved when $y(n) = a(n - K)$, i.e., $y(n)$ is perfect replica of $a(n)$ and is with a shift of K points. This removes both aliasing and distortion from the reconstruction. For two channel filter bank, the PR condition is given by

$$\begin{bmatrix} F_o(z) \\ F_1(z) \end{bmatrix} = \frac{2z^{-L}}{\Delta(z)} \begin{bmatrix} H_1(-z) \\ -H_o(-z) \end{bmatrix} \tag{34}$$

where $\Delta(z)$ is given by

$$\Delta(z) = H_o(z)H_1(-z) - H_o(-z)H_1(z) \tag{35}$$

The simplest implementation of this is the lazy filter bank, in which the first channel is detected without any modulation while the second channel shifts the input by one time step.

$$H_o(z) = 1 \;\; ; \;\; H_1(z) = z^{-1}$$

$$\Delta(z) = -2z^{-1} \;\; ; \;\; K = 1 \qquad (36)$$

$$F_o(z) = z^{-1} \;\; ; \;\; F_1(z) = 1$$

For the first case, $z = \exp\left(\frac{-j2\pi k}{2N+1}\right)$. Let total time of scan be $T = N\Delta t$. As only half of required number of points are scanned the phase modulation should be

$$\exp(j\phi(t)) = \exp\left(\frac{-j\pi t}{T}\right) \qquad (37)$$

This corresponds to a linear phase modulation from 0 to π phase shift in time T and thus the voltage provided by signal generator vary from 0 to V_π in this time. For large N (of the order of 10,000), the assumption that $\phi(t)$ varies slowly in Δt holds.

For the second case we assumed that the frequency of the modulation is comparable to c/l_o, which can be of the order of 10s of megahertz. It is difficult as well as cost ineffective to produce arbitrary waveforms at such high frequency. The easiest modulation is sinusoidal, produced using an RF signal generator.

$$\exp(j\phi(t)) = \exp(jA\sin(2\pi f_m t)) \qquad (38)$$

f_m is the sinusoidal phase modulation frequency and A is its amplitude. This gives

$$\bar{H}(i) = J_0\left(2A\sin\left(\frac{\pi f_m i l_o}{c}\right)\right) \qquad (39)$$

J_0 is the Bessel function of first kind and zeroth order. The corresponding filter coefficients and transfer function can be calculated from equation (31). To carry out the filter bank analysis, it is important that $\Delta(z)$ is invertible. For this purpose, the amplitude (A) and modulation frequency (f_m) can be engineered so as to make the analysis filter stable. Alternatively, other types of waveforms can be used, but that would require high speed analog waveform generators.